Confocal reflection readout thresholds in two-photon-induced optical recording

Xiangping Li, James W. M. Chon, and Min Gu*

Centre for Micro-Photonics, Faculty of Engineering and Industrial Sciences, Swinburne University of Technology,
P.O. Box 218, Hawthorn, Victoria 3122, Australia

*Corresponding author: mgu@swin.edu.au

Confocal reflection readout thresholds in two-photon-induced optical recording in photoisomerization polymer are studied both theoretically and experimentally. A threshold of the axial response from a planar reflector with a refractive-index change of the order of 10^{-2} is revealed. However, the threshold is reduced to 0.006 when strong forward scattering caused by the recorded bits leads to multiple reflection between the bit and the rare surface, which enhances the image contrast and reduces the readout threshold. The quality of the reconstructed bit image is strongly dependent on the refractive-index mismatch at the sample rare interface as well as the distance between the recorded position and the rare surface.   © 2008 Optical Society of America

OCIS codes: 110.3010, 180.1790.

1. Introduction

Two-photon (2P) excitation, generated by focusing through a high numerical aperture (NA) objective provides an effective method for inducing highly localized refractive-index change in polymers [1–10]. This technique has played an important role in many photonic applications including three-dimensional (3D) optical recording and data storage. It has been demonstrated that 2P excitation can induce the refractive-index change in a variety of materials, including photochromic, photorefractive, and photoisomerization materials [2–5,9–11], although the strength of the refractive-index change varies in those materials. Confocal reflection scanning microscopy is a powerful tool for the image reconstruction of the 3D refractive-index variation in a thick sample due to its nature of preventing the out-of-focus signal [12,13]. The 2P-induced refractive-index change in photochromic materials is of the order of 10^{-2} and has been successfully read out using confocal reflection microscopy [14–17]. 2P induced refractive-index

change in photorefractive polymers is typically less than 1%, and it has been demonstrated that confocal reflection readout exhibits a threshold of the writing power [18].

The 2P-induced refractive-index change ranges from 0.003 to 0.01 in the azo-dye-dispersed photoisomerization polymer [9–11,19–21]. It can be expected that the confocal reflection readout threshold in this case should highly depend on the recording power as well as the recorded structure shape. Here, we report on the confocal reflection readout thresholds in two cases in the azo-dye-dispersed photoisomerization polymer. One is the planar structures that are much larger than the wavelength of the reading beam [Fig. 1(a)], and the other is the array of bits that correspond to the focal size of a recording beam [Fig. 1(b)]. The axial response of the planar reflection model [Fig. 1(a)] is used to determine the confocal reflection readout threshold both theoretically and experimentally. A scattering model [Fig. 1(b)] is used to characterize confocal reflection readout of the 2P-induced refractive-index change, which reveals that the confocal reflection readout threshold is lower than that in the planar layer reflection model.
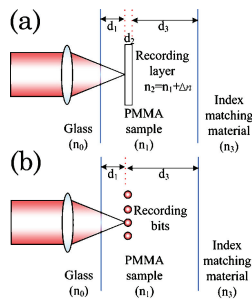
Fig. 1. (Color online) Experimental geometry. (a) Planar reflection readout. A planar reflection layer with refractive-index change Δn is recorded in an azo-dye-dispersed PMMA sample. The reflection is collected by an objective with NA = 1.4. (b) Scattering readout of recorded bits.

2. Confocal Reflection Readout Threshold in a Planar Reflection Model

A. Experiment

To record planar structures in a thick azo-dye-dispersed photoisomerization polymer, we prepared a poly(methyl methacrylate (PMMA) medium dispersed with 10 wt.% of Disperse Red 1 (DR1) and a thickness of $19 \pm 1\,\mu m$. The refractive index of the PMMA sample was measured to be 1.498 ± 0.002 using the traditional Becke line method with a serial of refractive-index liquids (Cargille Laboratories). A linearly polarized Ti:sapphire ultrashort pulsed laser beam of pulse width 100 fs and repetition rate 82 MHz (Spectra-Physics Tsunami) at a wavelength of 720 nm was employed as a light source for 2P excitation. A high NA objective (NA = 1.4) was used to focus the excitation on the sample to induce a layer of the refractive-index change [Fig. 1(a)] [9]. In such an experimental configuration, the support region of spatial frequencies partially overlaps the passband of the 3D coherent transfer function [2].

For confocal reflection microscopy, the same laser beam and objective were used for imaging. The reflected signal was focused by a lens with a focal length of 200 mm onto a pinhole with a diameter of $30\,\mu m$ in front of the photomultiplier tube. The axial response from the planar reflector scanned axially is a measure of the capability for axial imaging [22] and gives rise the threshold of the recoding power in confocal reflection readout. To readout the axial image of the recording layers, two immersion media were used. One sample was with air at the rare surface ($n_3 = 1.0$), and the other was with Norland 63 ($n_3 = 1.52$, Norland Products, Inc.) at the rare surface.

A planar reflector is recorded $5\,\mu m$ below the first surface by scanning a square of $10\,\mu m$ by $10\,\mu m$ in the sample with a power of 11 mW and an exposure time of $300\,ms/\mu m^2$. The transmission image of the recording layer is shown in Fig. 2(a). The axial images of the recording layer in the sample with the air rare surface are shown in Fig. 2(b). A similar experiment is performed in the sample with the Norland rare surface, as shown in Figs. 2(c) and 2(d). The first reflection peak corresponds to the coverglass ($n = 1.523$,
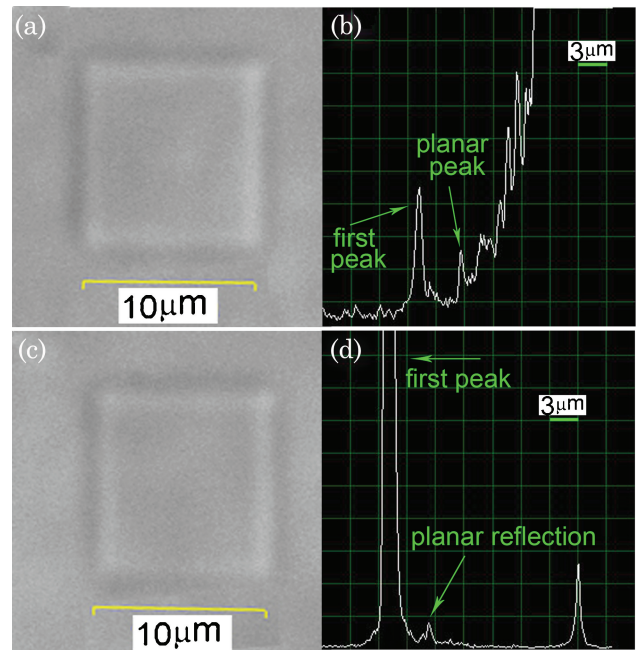

Fig. 2. (Color online) Experimental results of the axial image of the recording layer. (a) transmission and (b) axial images of the recording layer in the sample with air at the rare surface. (c) transmission and (d) axial images of the recording layer in the sample with Norland at the rare surface. The recording power is 11 mW. The scale bar in axial images is $3\,\mu m$.

Deckglaser)/PMMA sample interface, and the third peak corresponds to the PMMA sample/rare surface. Hereafter we call the former the first peak and the latter the main peak. The middle peak originates from the planar reflection of the recording layer. It is seen that the axial image can be read out when the refractive-index change is large enough.

To demonstrate the threshold effect of the axial response, the recording power is varied to produce planar reflectors with different index changes. The readout intensity of the planar reflection normalized to that from the front surface, which has a refractive-index mismatch of 0.025 and is detectable in the system, is shown as a function of the recording power in Fig. 3. There is a clear threshold effect on the axial response from the planar reflector of a small refractive-index change introduced by the DR1 molecules under 2P irradiance. Below a recording power of 11 mW, the refractive-index change is too small to introduce any resolvable axial image response. Above that, the reflection from the refractive-index change layer can be resolved, which corresponds to a calculated refractive-index change of 10^{-2}. In particular, the intensity of the axial response increases dramatically when the deformation of PMMA is observed. This threshold effect is consistent with previous results [2,18].

B. Theory

To confirm the observation in Figs. 2 and 3, we consider an aberration-free confocal reflection system, when a planar object is scanned along the axis
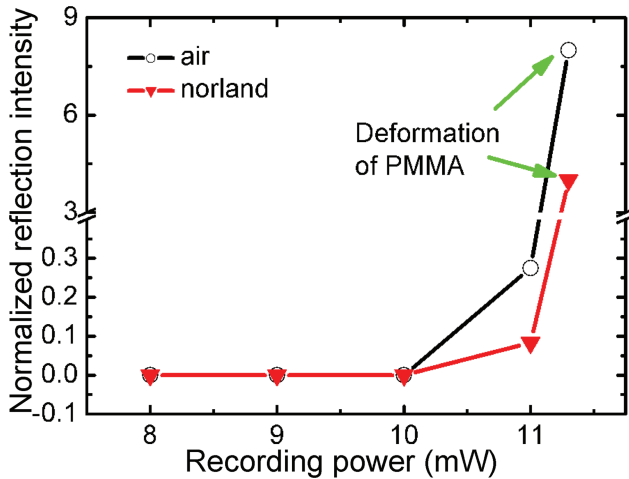
Fig. 3. (Color online) Experimental readout of the confocal reflection intensity normalized to the reflection intensity of the front surface as a function of the recording power. The circle and triangle are the sample with air and Norland at the rare surface, respectively.

[12,22]. The detected reflection intensity as a function of the defocused distance z can be written as [22,23]

$$I(z) = |\int_0^a r(\theta) \exp(2ikn_0 z \times \cos\theta) \sin\theta \times \cos\theta d\theta|^2, \quad (2.1)$$

where $r(\theta)$ is the reflection coefficient for the planar structure. For linear polarized illumination, the effective reflection coefficient for parallel and perpendicular polarization is given by [22]

$$r(\theta) = (r_\sigma - r_\pi)/2. \quad (2.2)$$

According to Born and Wolf [24], the reflection coefficient for the beam through a three-layer structure is

$$r_{\sigma/\pi} = \frac{r_{01\sigma/\pi} + r_{12\sigma/\pi} \exp(2ikn_x d_x \cos\theta_x)}{1 + r_{01\sigma/\pi} r_{12\sigma/\pi} \exp(2ikn_x d_x \cos\theta_x)}, \quad (2.3)$$

where r_{01} and r_{12} are reflection coefficients of the first interface and the second interface, respectively. n_x and d_x are the refractive index and the thickness of the middle medium, respectively. θ_x is the refracted angle of the beam inside the middle medium from the normal to the front surface.

For the experiment configuration as shown in Fig. 1 (a), the sample can be treated as a five-layer structure. The reflection coefficients for each interface can be given as

$$r_{01\sigma} = \frac{n_0 \cos\theta_0 - n_1 \cos\theta_1}{n_0 \cos\theta_0 + n_1 \cos\theta_1}, \quad (2.4)$$

$$r_{01\pi} = \frac{n_1 \cos\theta_0 - n_0 \cos\theta_1}{n_1 \cos\theta_0 + n_0 \cos\theta_1}, \quad (2.5)$$

$$r_{12\sigma} = \frac{n_1 \cos\theta_1 - n_2 \cos\theta_2}{n_1 \cos\theta_1 + n_2 \cos\theta_2}, \quad (2.6)$$

$$r_{12\pi} = \frac{n_2 \cos\theta_1 - n_1 \cos\theta_2}{n_2 \cos\theta_1 + n_1 \cos\theta_2}, \quad (2.7)$$

$$r_{23\sigma} = \frac{n_2 \cos\theta_2 - n_1 \cos\theta_3}{n_2 \cos\theta_2 + n_1 \cos\theta_3}, \quad (2.8)$$

$$r_{23\pi} = \frac{n_1 \cos\theta_2 - n_2 \cos\theta_3}{n_1 \cos\theta_2 + n_2 \cos\theta_3}, \quad (2.9)$$

$$r_{34\sigma} = \frac{n_1 \cos\theta_3 - n_3 \cos\theta_4}{n_1 \cos\theta_3 + n_3 \cos\theta_4}, \quad (2.10)$$

$$r_{34\pi} = \frac{n_3 \cos\theta_3 - n_1 \cos\theta_4}{n_3 \cos\theta_3 + n_1 \cos\theta_4}. \quad (2.11)$$

Substituting Eqs. (2.4), (2.5), (2.6), (2.7), (2.8), (2.9), (2.10), and (2.11) into Eq. (2.3), we can derive the total reflection coefficient of the five-layer structure. This rigorous theory incorporates the depletion of the incident beam as it travels through the structure, aberration caused by focusing through the refractive media, as well as multiple reflections [22,23].

To study the reflection intensity from a planar reflector with a small refractive-index change in front of a large refractive-index mismatched interface, we show in Fig. 4 the numerical analysis of the axial response from the five-layer structure by variation of the refractive index n_3 of the matching materials at the rare surface. Figures 4(a)/4(b), 4(c)/4(d), 4(e)/4 (f), 4(g)/4(h) are the reflection from the sample when air, water ($n_3 = 1.33$), Norland, and PMMA samples ($n_3 = n_1$) are at the rare surface, respectively. The right column is the zoom in view of the left column. The refractive-index change of the planar reflector is assumed to be 0.005, recorded 5 μm below the front surface of the sample of a thickness of 0.3 μm and $d_3 = 13 \mu$m.

Three peaks are expected, corresponding to the reflection from the front surface, the planar reflector, and the rare surface. It is clear that when there is
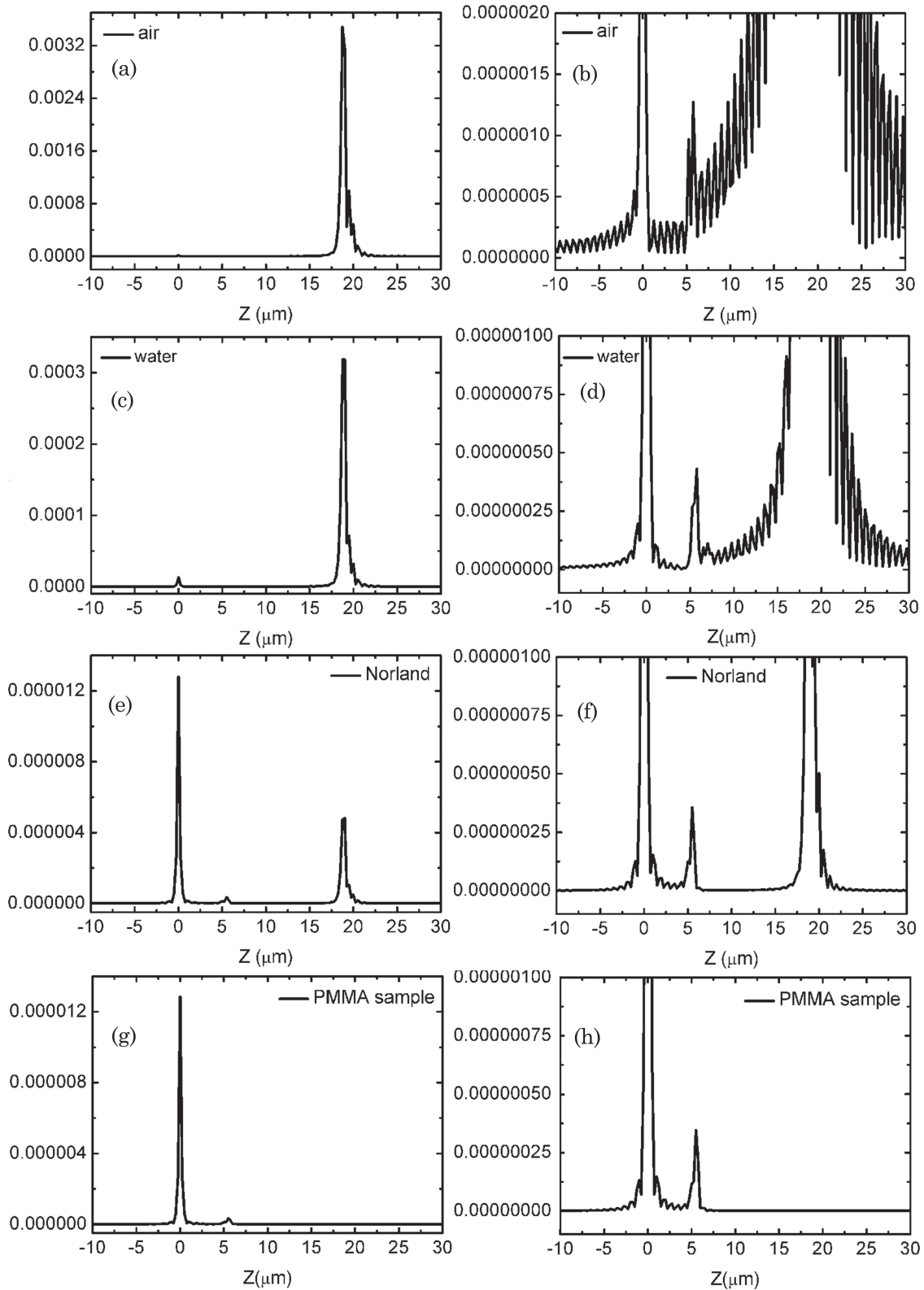
Fig. 4. Theoretical calculation of the confocal axial response from the planar reflector with an index change of 0.005. The reflector is $5\,\mu m$ below the front surface. (a)/(b), (c)/(d), (e)/(f), and (g)/(h) are samples with air, water, Norland, and PMMA ($n_3 = n_1$) at the rare surface, respectively. The right column is a zoom-in view of the left column.

refractive-index mismatching at the front surface, the main peak loses its symmetry due to the aberration. There is no reflection from the rare surface when the refractive index is completely matched as shown in Figs. 4(g) and 4(h). The sidelobes on the right side of the main peak are dominated by

phase aberration, which is determined by the refractive-index mismatch at the front surface. As we increase the refractive index n_3 of the matching materials at the rare surface to match the PMMA sample, the strength of sidelobes in the backwards direction, dominated by multiple reflection, is reduced. In the meantime the absolute reflection intensity from the planar reflector is also reduced due to the exclusion of the multiple reflection contribution [see Figs. 4(c)–4(f)].

To study the threshold effect of the axial response from the planar reflector, the theoretical calculations of the planar reflection for the samples with the air rare surface and the Norland rare surface are plotted as a function of the refractive index in Fig. 5. As the reflection from the front surface is approximately constant in both samples, the planar reflection intensity is normalized to that from the front surface. It is clear that for the sample with the air rare surface the planar reflection is stronger than that for the sample with the Norland rare surface. Below the refractive-index change of 0.01, the reflection is weak and barely resolvable. Above the refractive-index change of 0.1, corresponding to the deformation of the polymer matrix, the strength of the axial response is increased dramatically. The axial response threshold effect predicted by the theoretical calculation is consistent with the experimental observation that a refractive-index change of 0.01 or above, corresponding to the recording power of 11 mW or higher, is required.

3. Confocal Reflection Readout Threshold in a Bit Scattering Model

Now let us turn to an alternation structure where an array of bits is recorded in a thick medium [Fig. 1(b)]. The recording and confocal reading system is the same as described before. A pattern consisting of 9 by 9 bits with a bit spacing of $1.5\,\mu$m was recorded at $14\,\mu$m below the front surface. The recording

power is 10 mW, and the exposure time for each bit is fixed at 25 ms, corresponding to $200\,\text{ms}/\mu\text{m}^2$. We scanned the sample in the axial direction and no confocal reflection signal from the refractive-index change of the recorded bits could be detected near the recording depth position However, the image of the recorded pattern can be reconstructed at the other positions through the multiple reflections between the strong forward scattering of bits and the rare surface. Figures 6(a) and 6(b) show the reflection images reconstructed at $10.3\,\mu$m and $15\,\mu$m below the front surface, respectively. The readout contrast of the bits is plotted as a function of the reading depth below the front surface, as shown in Fig. 6(c). The readout contrast profile has two broad peaks shifting away from the recording position with a central position at $10.3\,\mu$m and $15\,\mu$m, respectively. A possible explanation for the origin of two peaks is the interference between the forward scattering and the multiple reflections, which forms the interference fringes [25]. From Eq. (2.1) the phase of the reflected signal is dependent on the angle of the ray, which leads to the shift of the reflection peaks by approximately $0.5\,\mu$m, shown in Figs. 4(a)–4(f). Similarly the angular dependence of the phase of the reflected forward scattering causes the shift of the peak away from the recording position.

To characterize the reconstructed image induced by bit scattering, the pattern was recorded at different depths and readout slice by slice. The readout contrast is plotted as a function of distance d_3 [see Fig. 2(b)] between the recorded position and the rare surface, as shown in Fig. 7(a). As d_3 gradually reduces, the confocal reflection readout contrast increases dramatically due to the increased strength of multiple reflection between the forward scattering of bits and the rare surface. This observation is confirmed by changing the matching medium. The
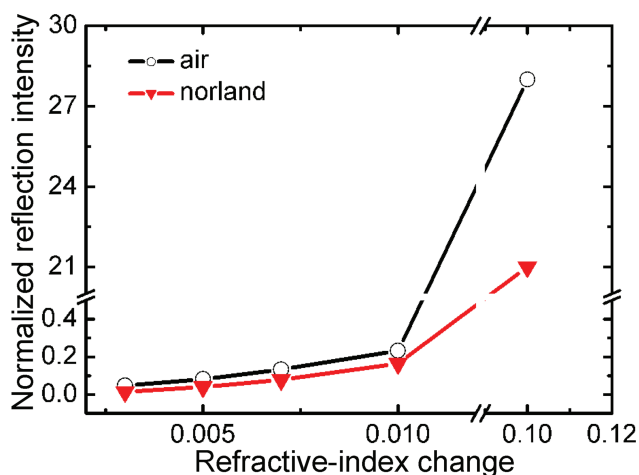

Fig. 5. (Color online) Theoretical calculation of the confocal reflection intensity of the planar reflector normalized to the reflection intensity of the front surface as a function of the refractive-index change. The circle and triangle are the sample with air and Norland at the rare surface, respectively.
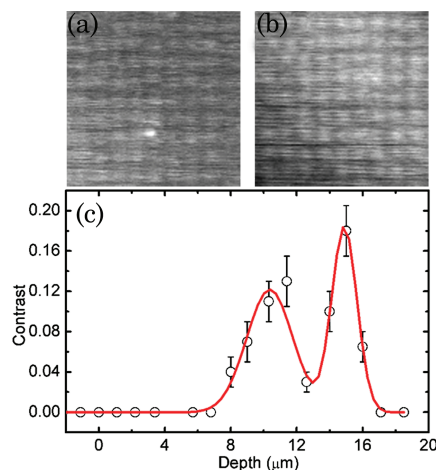

Fig. 6. (Color online) Scattering-induced reflection image reconstruction. (a), (b), and (c) are the scattering-induced reflection images of recorded bits read out at $10.3\,\mu$m and $15\,\mu$m below the front surface, respectively. The recording power is 10 mW and the exposure time is $200\,\text{ms}/\mu\text{m}^2$. (c) Readout contrast of the recorded bits as a function of the reading position.

Fig. 8. (Color online) Scattering-induced readout contrast of the recorded bits as a function of the recording power in the sample with air at the rare surface.
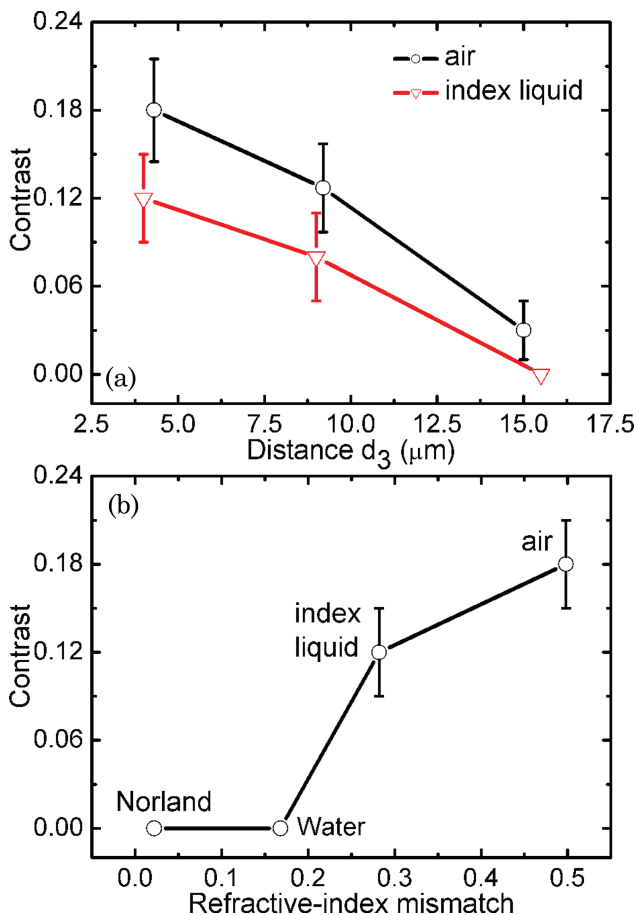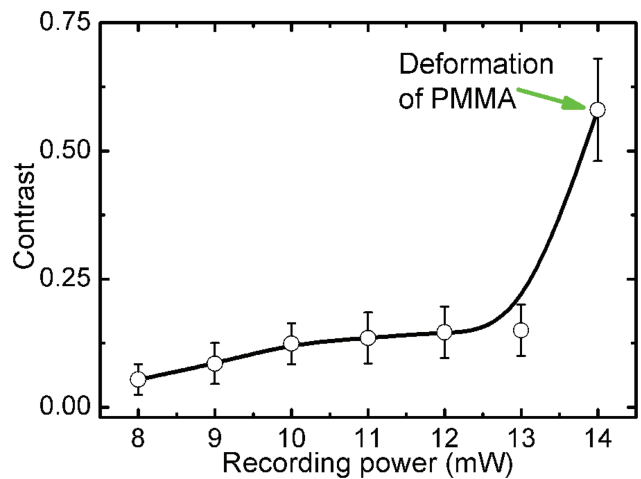
Fig. 7. (Color online) (a) Reflection image contrast as a function of the distance between the recording position and the rare surface. The circle and triangle are the samples with air and liquid at the rare surface, respectively. (b) Reflection image contrast as a function of the refractive-index mismatch at the rare surface.

image of the recorded pattern cannot be read out in the sample with Norland or water at the rare surface no matter the distance d_3. As shown in Figs. 4(c)–4(f) multiple reflections become weak, therefore reducing the interference of scattering beam with multiple reflections. Since multiple reflections from the rare surface are enhanced as the refractive index of the mismatching medium increases, a liquid medium with a refractive index of $n = 1.78$ (Cargille Laboratories) was placed at the rare surface. The image of recorded bits can be reconstructed and the corresponding reflection image contrast as a function of d_3 is shown in Fig. 7(a). Figure 7(b) shows the reflection image contrast as a function of the refractive index of the mismatching media at the rare interface. It is clear that the scattering-induced reflection image contrast is enhanced as the increase in the mismatching refractive-index at the rare surface.

Figure 8 shows the confocal reflection readout contrast as a function of the recording power in the sample with air at the rare surface. The recorded position was fixed at $14\,\mu m$ below the front surface and exposure time was fixed at $25\,ms$ for each bit. Generally,

the recorded bits can be read out when the recording power is above $8\,mW$, corresponding to calculated refractive-index change of 0.006. As we gradually increase the recording beam intensity, the readout contrast is enhanced. The readout contrast increases dramatically as the recording power is above $13\,mW$ when the deformation of PMMA occurs.

4. Conclusion

Axial images of the 2P-induced refractive-index change in the azo-dye-dispersed PMMA sample has been investigated both theoretically and experimentally in confocal microscopy. A confocal reflection readout threshold of the axial response from a planar reflector with a refractive-index change of the order of 10^{-2} is revealed. However, the threshold is reduced when the recoded pattern is composed of an array of bits. The strong forward scattering caused by the bits leads to multiple refection between the bit and the rare surface, which enhances the image contrast and reduces the readout threshold. The quality of the reconstructed bit image is strongly dependent on the refractive-index mismatch at the sample rare interface as well as the distance between the recorded position and the rare surface.

References
1. D. A. Parthenopoulos and P. M. Rentzepis, "Three-dimensional optical storage memory," Science **245**, 843–845 (1989).
2. A. Toriumi, S. Kawata and M. Gu, "Reflection confocal microscope readout system for three-dimensional photochromic optical data storage," Opt. Lett. **23**, 1924–1926 (1998).
3. J. H. Strickler and W. W. Webb, "Three-dimensional optical data storage in refractive media by two-photon point excitation," Opt. Lett. **16**, 1780–1782 (1991).
4. Y. Kawata, H. Ishitobi, and S. Kawata, "Use of two-photon absorption in a photorefractive crystal for three-dimensional optical memory," Opt. Lett. **23**, 756–758 (1998).
5. D. Day, M. Gu, and A. Smallridge, "Use of two-photon excitation for erasable rewritable three-dimensional bit optical data

storage in a photorefractive polymer," Opt. Lett. **24**, 948–950 (1999).

6. D. McPhail and M. Gu, "Use of polarization sensitivity for three-dimensional optical data storage in polymer dispersed liquid crystals under two-photon illumination," Appl. Phys. Lett. **81**, 1160–1162 (2002).

7. J. W. M. Chon, P. Zijlstra, M. Gu, J. van Embden, and P. Mulvaney, "Two-photon-induced photoenhancement of densely packed CdSe/ZnSe/ZnS nanocrystal solids and its application to multilayer optical data storage," Appl. Phys. Lett. **85**, 5514–5516 (2004).

8. X. Li, Bullen. C, J. W. M. Chon, R. A. Evans, and M. Gu, "Two-photon-induced three-dimensional optical data storage in CdS quantum-dot doped photopolymer," Appl. Phys. Lett. **90**, 161116 (2007).

9. X. Li, J. W. M. Chon, S. Wu, R. A. Evans, and M. Gu, "Rewritable polarization-encoded multilayer data storage in 2,5-dimethyl-4-(p-nitrophenylazo)anisole doped polymer," Opt. Lett. **32**, 277–279 (2007).

10. X. Li, J. W. M. Chon, R. A. Evans, and M. Gu, "Two-photon energy transfer enhanced three-dimensional optical memory in quantum-dot and azo-dye doped polymers," Appl. Phys. Lett. **92**, 063309 (2008).

11. M. Maeda, H. Ishitobi, Z. Sekkat, and S. Kawata, "Polarization storage by nonlinear orientational hole burning in azo dye-containing polymer films," Appl. Phys. Lett. **85**, 351–353 (2004).

12. M. Gu, *Principles of Three-Dimensional Imaging in Confocal Microscopes* (World Scientific, 1996), pp. 1–3.

13. C.J. R. Sheppard, M. Gu, and X. Q. Mao, "Three-dimensional coherent transfer function in a reflection-mode confocal scanning microscope," Opt. Commun. **81**, 281–284 (1991).

14. T. Wilson, Y. Kawata, and S. Kawata, "Readout of three-dimensional optical memories," Opt. Lett. **21**, 1003–1005 (1996).

15. M. Gu, "Confocal readout of three-dimensional data bits recorded by the photorefractive effect under single-photon and two-photon excitation," Proc. IEEE **87**, 2021–2029 (1999).

16. M. Gu, J. O. Amistoso, A. Toriumi, M. Irie, and S. Kawata, "Effect of saturable response to two-photon absorption on the readout signal level of three-dimensional bit optical data storage in a photochromic polymer," Appl. Phys. Lett. **79**, 148–150 (2001).

17. S. Kawata and Y. Kawata, "Three-dimensional optical data storage using photochromic materials," Chem. Rev. **100**, 1777–1788 (2000).

18. D. Day and M. Gu, "Formation of voids in a doped polymethylmethacrylate polymer," Appl. Phys. Lett. **80**, 2404–2406 (2002).

19. T. Hattori, T. Shibata, S. Onodera, and T. Kaino, "Fabrication of refractive index grating into azo-dye-containing polymer films by irreversible photoinduced bleaching," J. Appl. Phys. **87**, 3240–3244 (2000).

20. M. Ivanov, T. Todorov, L. Nikolova, N. Tomova, and V. Dragostinova, "Photoinduced change in the refractive index of azo-dye/polymer systems," Appl. Phys. Lett. **66**, 2174–2176 (1995).

21. Z. Sekkat, H. Ishitobi, and S. Kawata, "Two-photon isomerization and orientation of photoisomers in thin films of polymer," Opt. Commun. **222**, 269–276 (2003).

22. C. J. R. Sheppard and M. Gu, "Axial imaging through an aberrating layer of water in confocal microscopy," Opt. Commun. **88**, 180–190 (1992).

23. C. J. R. Sheppard, M. Gu, K. Brain, and H. Zhou, "Influence of spherical aberration on axial imaging of confocal reflection microscopy," Appl. Opt. **33**, 616–624 (1994).

24. M. Born and E. Wolf, *Principles of Optics*, 5th ed. (Pergamon, 1975), pp. 100–108.

25. D. Ganic, X. Gan, and M. Gu, "Near-field imaging by a micro-particle: a model for conversion of evanescent photons into propagating photons," Opt. Express. **12**, 5325–5335 (2004).